JOURNAL OF SYNCHROTRON RADIATION
ISSN 1600-5775

Microbubbles containing gadolinium as contrast agents for both phase contrast and magnetic resonance imaging

Rongbiao Tang,[a]* Fuhua Yan,[a] Guo-Yuan Yang[b] and Ke-Min Chen[a]*

[a]Department of Radiology. Rui Jin Hospital, Shanghai Jiao Tong University School of Medicine, Shanghai 200025, People's Republic of China, and [b]Neuroscience and Neuroengineering Center, Med-X Research Institute, Shanghai Jiao Tong University, Shanghai 200030, People's Republic of China. *Correspondence e-mail: tangme8688258@sina.com, keminchenrj@163.com

Received 9 October 2017
Accepted 4 December 2017

Edited by P. A. Pianetta, SLAC National Accelerator Laboratory, USA

Keywords: phase contrast imaging; microbubble; gadolinium.

Portal vein imaging is an important method for investigating portal venous disorders. However, the diagnostic requirements are not usually satisfied when using single imaging techniques. Diagnostic accuracy can be improved by combining different imaging techniques. Contrast agents that can be used for combined imaging modalities are needed. In this study, the feasibility of using microbubbles containing gadolinium (MCG) as contrast agents for both phase contrast imaging (PCI) and magnetic resonance imaging (MRI) are investigated. MCG were made by encapsulating sulfur hexafluoride (SF_6) gas with gadolinium and lyophilized powder. Absorption contrast imaging (ACI) and PCI of MCG were performed and compared *in vitro*. MCG were injected into the main portal trunk of living rats. PCI and MRI were performed at 2 min and 10 min after MCG injection, respectively. PCI exploited the differences in the refractive index and visibly showed the MCG, which were not detectable by ACI. PCI could facilitate clear revelation of the MCG-infused portal veins. The diameter of the portal veins could be determined by the largest MCG in the same portal vein. The minimum diameter of clearly detected portal veins was about 300 µm by MRI. These results indicate that MCG could enhance both PCI and MRI for imaging portal veins. The detection sensitivity of PCI and MRI could compensate for each other when using MCG contrast agents for animals.

1. Introduction

Nowadays, many imaging methods, such as ultrasound imaging, fluorescence imaging, computed tomography (CT), magnetic resonance imaging (MRI) and phase contrast imaging (PCI), have been developed for noninvasive diagnosis and biomedical applications (Kim *et al.*, 2013; Bravin *et al.*, 2013; Beekman & Hutton, 2007; Ao *et al.*, 2010). Portal vein imaging is commonly performed using these imaging techniques. However, each of these imaging modalities has its own advantages and limitations in areas such as resolution, sensitivity, scanning speed and penetration depth (Sciallero *et al.*, 2016; Gregg & Butcher, 2012; Chiriacò *et al.*, 2013). Considerable improvement can be obtained by combining two or more imaging techniques simultaneously. Different imaging techniques function through different principles and thus use different contrast agents (Chen *et al.*, 2012; Ao *et al.*, 2010). Therefore, it is crucial to have contrast agents that can be simultaneously used in several imaging techniques.

MRI is a multi-parameters imaging method; it can offer much diagnosis information (Zhang *et al.*, 2008; Huang *et al.*, 2016). Contrast-enhanced MRI is generally applied to diagnose soft tissue and vascular abnormalities. Currently, gado-

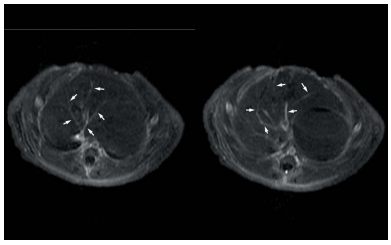

linium is clinically used as a T1-weighted imaging (T1WI) contrast agent. The longitudinal relaxation time (T1) of protons can be distinctly shortened by gadolinium. Post-gadolinium T1WI can be applied to opacify blood vessels and identify abnormal enhancement.

Physiological saline is clinically used to dissolve lyophilized powder. Then the solution is employed to coat sulfur hexafluoride (SF_6) gas to produce microbubbles. The microbubbles are commonly used as ultrasound contrast agents (Claudon *et al.*, 2008). In addition, microbubbles can also be considered as suitable contrast agents for synchrotron radiation (SR) imaging (Jamison *et al.*, 2011; Lee *et al.*, 2014; Millard *et al.*, 2015; Tang *et al.*, 2016). Because the SF_6 gas has a different refractive index from the surrounding tissues, distinct phase shifts can be obtained at the gas–tissue interfaces (Tang *et al.*, 2011). According to the phase shifts, PCI can enable the clear visibility of the boundaries (Tang *et al.*, 2011, 2017; Xi *et al.*, 2011). Hence, the SF_6 gas–vascular wall interfaces can be highly delineated on phase contrast images to show blood vessels.

In this study, we created microbubbles containing gadolinium (MCG). MCG were injected into the hepatic portal veins of living rats. The aim of this study was to evaluate the feasibility of using MCG as contrast agent for both PCI and MRI in living rats.

2. Materials and methods

2.1. MCG preparation

The effects of MCG as contrast agents for both PCI and MRI were evaluated by hepatic portal venography. 2 ml gadolinium (BEILU, China) was injected into a vial of lyophilized powder (SonoVue, Switzerland) (Fig. 1). Then the vial was shaken to make sure that the powder was fully dissolved. The solution was evenly mixed to encapsulate SF_6 gas to produce MCG. MCG were placed on glass coverslips and imaged under a light microscope using a 200× magnification.

2.2. SR parameters

PCI was carried out at the BL13W1 beamline at Shanghai Synchrotron Radiation Facility (SSRF), People's Republic of China. SR beams were created using a 3.5 GeV electron storage ring. The beamline had an energy range of 8–72.5 keV. The energy resolution ($\Delta E/E$) was less than 5×10^{-3}. The original SR beams were monochromated using a double-crystal monochromator with Si(111) and Si(311) crystals. The transmitted beams were captured by a 100 µm-thick $CdWO_4$ cleaved single-crystal scintillator and transformed to observable images. Samples were positioned 34 m downstream of the synchrotron source. The sample-to-detector distance (SDD) was adjustable with a range of 8 m. A diagram of the setup is given in Fig. 2.

Figure 1
Production materials for MCG. 2 ml gadolinium was added to dissolve lyophilized powder. Then SF_6 gas was encapsulated by the mixture to make MCG.

2.3. Comparison between absorption contrast imaging (ACI) and PCI

MCG were placed in a PE-50 catheter that was set perpendicular to the SR beam. Based on the imaging principles of in-line PCI, phase and absorption contrast information can be chosen by changing the SDD (Snigirev *et al.*, 1995; Wilkins *et al.*, 1996). ACI can be attained with an SDD near 0. Thus the SDDs for ACI and PCI were set to 5 mm and 30 cm, respectively. Except for the SDD, the other imaging parameters for ACI and PCI were the same.

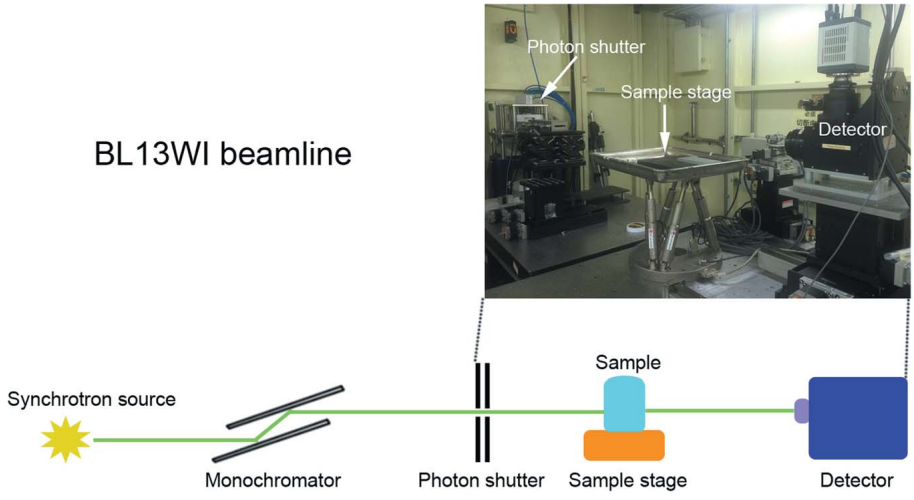

Figure 2
Schematic of the imaging setup at BL13W1 at SSRF. The distance between synchrotron source and sample stage was 34 m. The inset shows the imaging equipment in the experimental hutch. The distance between the photon shutter and sample stage was 1.7 m. The SDD could be changed from 0 to 8 m by moving the detector on the rail.

2.4. PCI of portal veins with MCG

All animal experiments were performed in accordance with guidelines for the care and use of laboratory animals of Shanghai Jiao Tong University (SJTU). The experimental protocols were approved by the Institutional Animal Care and Use Committee (IACUC) and the Bioethics Committee of the School of Medicine, SJTU. Eight male Sprague Dawley rats (Animal Center, CAS, Shanghai) weighing 150–160 g were used. Five rats were used for PCI; the other three rats were used for MRI. All rats were kept in a temperature-controlled room with a 12 h light–dark cycle. They had free access to water and a normal diet in a pathogen-free environment. Rats were anesthetized with ketamine (100 mg kg^{-1}) and xylazine (10 mg kg^{-1}) intraperitoneally. A mid-line abdominal incision was made after the rats were anesthetized. The main portal trunk was punctured with a thin PE-10 catheter through the mid-line laparotomy. Part of the hepatic lobe was protruded from the abdomen to obtain a direction perpendicular to the SR beams. 0.4 ml MCG solution was injected into the portal system through the catheter. At 2 min after the injection, PCI was performed at an energy level of 19 keV. The detector was placed at a distance of 30 cm from the liver.

2.5. MRI

The main portal trunk of the rats was intubated as described above. Rats were scanned using a clinical MRI unit operating at 3 T (GE, USA). Ten minutes after the MCG solution was injected into the portal system, a T1WI sequence was performed. Parameters were as follows: TR, 60 ms; TE, 14 ms; FOV, 12 cm; NEX, 4.00; section thickness, 1.5 mm.

3. Results

3.1. *In vitro* SR imaging of MCG

MCG were observed by optical microscopy. They were spherical microbubbles with smooth surfaces (Fig. 3). To confirm the superiority of PCI for showing the MCG, PCI was compared with ACI. Due to their low density, the MCG floated and located along the upper edge of the PE-50 catheter. When the MCG were imaged by ACI, they were poorly detected (Fig. 4*a*). PCI, by contrast, presented a clear visualization of the MCG (Fig. 4*b*). The MCG produced a more pronounced change in gray value with PCI (Fig. 4*d*) than with ACI (Fig. 4*c*).

3.2. PCI of hepatic portal veins with MCG *in vivo*

The MCG were injected into the portal veins before imaging, which meant that the portal system filled with MCG instead of blood. The MCG had a refractive index quite different from liver parenchyma. PCI exploited the differences in the refractive index and facilitated clear visualization of the MCG. Then the portal veins filled with MCG were indirectly shown. Many portal veins could be noticeably delineated by MCG (Figs. 5 and 6). The diameter of the MCG could be measured by identifying the density curve (Fig. 5*c*). Different sizes of MCG were found in the same portal vein. The diameter of the portal vein was determined by the largest MCG. In Figs. 6(*b*) and 6(*c*) the diameter of the largest MCG (green line) could be measured to obtain the diameter of the portal vein.

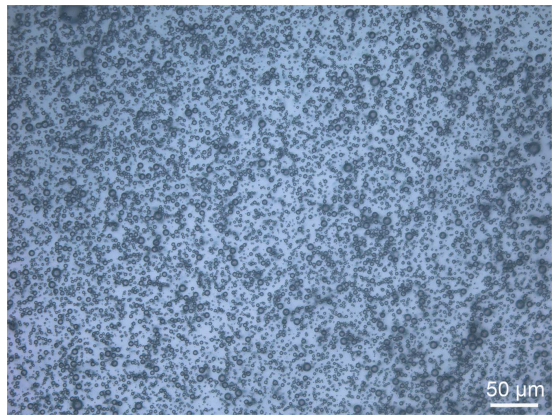

Figure 3
High-power micrograph of MCG. A light microscope showed that MCG were spherical particles with smooth surfaces. Original magnification: 200×.

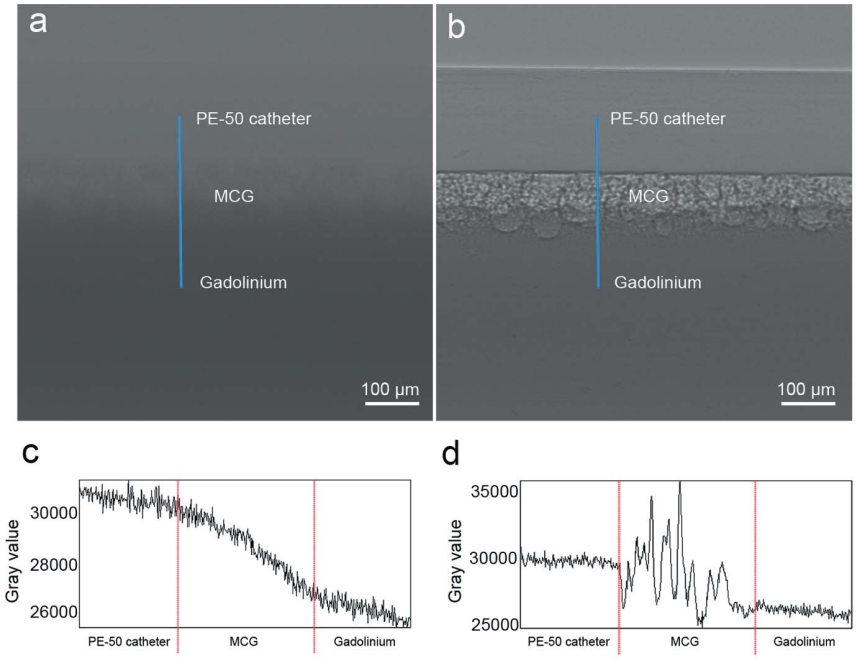

Figure 4
SR imaging of MCG and line profile analysis. PCI (*b*) showed the MCG more clearly than ACI (*a*). Line profile analyses of (*a*) and (*b*) are shown in (*c*) and (*d*), respectively. The gray values along the blue lines are displayed. Note that the MCG caused a distinct change in intensity (*d*) on the phase contrast image. The images were obtained with an SDD of 1 cm (*a*) and 30 cm (*b*). The pixel size was 1.625 µm × 1.625 µm, and the exposure time was 4 s.

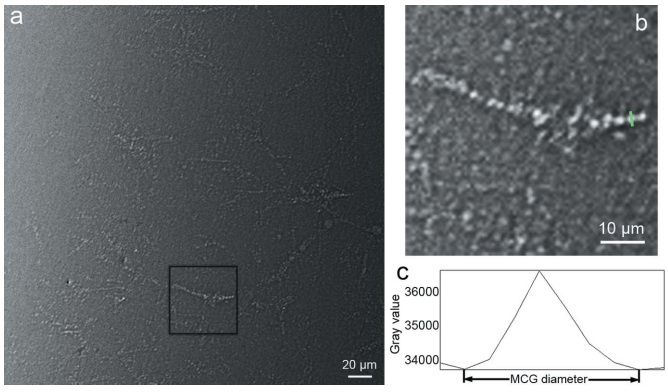

Figure 5
PCI of portal veins and measurement. Panel (*b*) is a magnified image of the region in the black box in (*a*). Portal veins filled with MCG could be evidently delineated. Panel (*c*) shows the gray value along the green line in (*b*). The MCG diameter could be measured by identifying the density curve. The images were obtained with an SDD of 30 cm. The pixel size was 0.325 μm × 0.325 μm, and the exposure time was 3 s.

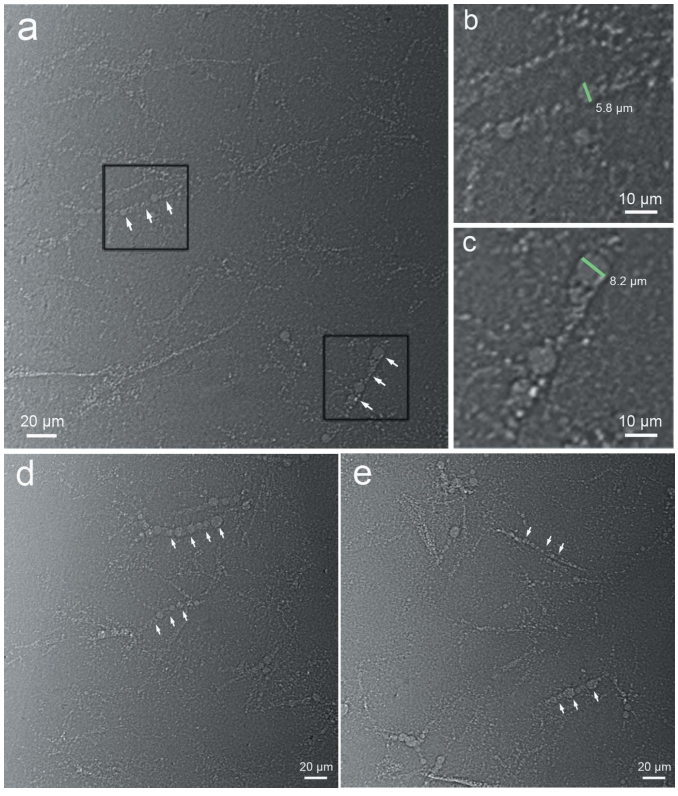

Figure 6
Representative phase contrast images of portal veins after MCG injection. Many portal veins (arrows) filled with MCG can be detected in panels (*a*), (*d*) and (*e*). Panels (*b*) and (*c*) are magnified images of the region in the black box in (*a*). Different sizes of MCG were found in the same portal vein. The diameter of the portal vein was determined by the largest MCG (green line), which could be measured by identifying the density curve as shown in Fig. 5(*c*). The images were obtained with an SDD of 30 cm. The pixel size was 0.325 μm × 0.325 μm and the exposure time was 3 s.

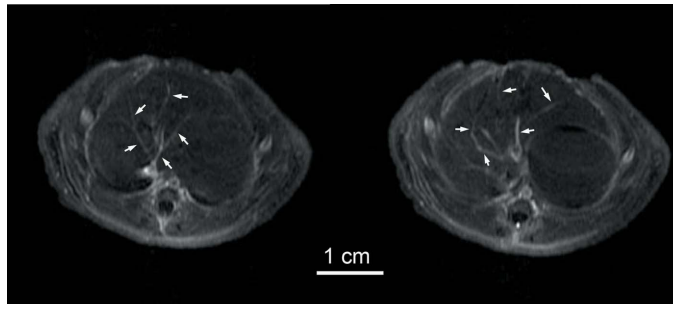

Figure 7
MRI of portal veins after MCG injection. Note that the portal branches (arrows) could be clearly delineated using MCG as T1WI contrast agents.

3.3. MRI of hepatic portal veins with MCG *in vivo*

Due to the gadolinium component, MCG solution could markedly shorten the longitudinal relaxation time (T1) of protons in blood, and brightened the portal veins where the agents were present. The portal branches (arrows) could be plainly shown (Fig. 7). The minimum diameter of clearly delineated portal veins was about 300 μm.

4. Discussion

Microbubbles exist in the form of solution in principle. SF_6 gas and lyophilized powder existed separately before adding the gadolinium. Gadolinium was found to be able to dissolve the lyophilized powder to form shell material. Microbubbles were made by encapsulating the SF_6 gas with the shell material. The perfusion would be stopped when the diameter of the MCG was equal to that of the portal vein. Therefore, the diameter of the portal vein can be determined by the largest MCG in the same vessel, as shown in Fig. 6.

MRI has been identified to have direct multi-planarity and high-quality soft tissue resolution (Honda, 2003; Qi *et al.*, 2016). The longitudinal relaxation time (T1) of protons was noticeably shortened by the gadolinium component from the MCG solution. Therefore, the MCG-filled portal veins could be clearly presented on T1WI. However, MRI has a relatively low resolution. ACI mainly reveals the absorption of X-rays between the adjacent materials. MCG contain a gas core, which absorbs the SR beam weakly, making MCG minimally detectable on ACI. By contrast, PCI principally utilizes phase shifts as contrast mechanisms (Lewis, 2004; Lundström *et al.*, 2014; Tang *et al.*, 2013). The introduction of MCG into vessels produces a significant change in the refractive index. The large difference in refractive index between the gas core of MCG and the surrounding tissues can produce considerable phase shifts. PCI exploits these phase shifts to greatly improve the image contrast at the gas core–tissue interfaces (Lee *et al.*, 2014; Tang *et al.*, 2011; Xi *et al.*, 2011). Therefore, due to the gas core, MCG can be considered as a suitable PCI contrast agent. By using a high-resolution detector, fine portal veins can be clearly shown. So PCI can supplement the relatively low resolution of MRI. In addition, it should be pointed out that we used projection PCI to obtain two-dimensional images of the portal veins. The portal veins that were perpendicular to

the SR beams could be clearly delineated. However, the portal veins could not be entirely shown if they were nearly parallel to the beams. In order to resolve this problem, PCI CT may be utilized to provide a three-dimensional visualization of the MCG-filled portal veins without overlapping in further research.

PCI and MRI were carried out at 2 min and 10 min after MCG injection, respectively. The portal veins were clearly shown using both imaging methods at the corresponding time point after injection. PCI and MRI may be capable of imaging the same rat with a single dose of MCG. Single utilization of contrast agents can reduce the potential side effects. It is more convenient and safer than administering these contrast agents separately.

In conclusion, MCG could be clearly identified from the surrounding tissues on both PCI and MRI. PCI could clearly detect the MCG-filled portal veins of several micrometers in diameter. MRI could provide multi-planar images with high-quality soft tissue resolution. One disadvantage of this study is that gadolinium was co-present in the solution (but not attached) with the microbubbles. However, the results still show that PCI can clearly detect microbubbles if they are coupled with gadolinium. At the present stage, PCI can be applied for animal imaging before its clinical use. Therefore, PCI and MRI can perfectly compensate each other by using MCG as contrast agents for animals.

Funding information

Funding for this research was provided by: National Natural Science Foundation of China (grant Nos. 81471808, 81271740, 81301347); National Basic Research Program of China (973 Program grant No. 2010CB834305); Shanghai Jiao Tong University Med-Science Cross Research Foundation (grant No. YG2013MS30).

References

Ao, M., Wang, Z., Ran, H., Guo, D., Yu, J., Li, A., Chen, W., Wu, W. & Zheng, Y. (2010). *J. Biomed. Mater. Res.* **93B**, 551–556.
Beekman, F. & Hutton, B. F. (2007). *Eur. J. Nucl. Med. Mol. Imaging*, **34**, 1410–1414.
Bravin, A., Coan, P. & Suortti, P. (2013). *Phys. Med. Biol.* **58**, R1–R35.
Chen, H., Rogalski, M. M. & Anker, J. N. (2012). *Phys. Chem. Chem. Phys.* **14**, 13469–13486.
Chiriacò, F., Soloperto, G., Greco, A., Conversano, F., Ragusa, A., Menichetti, L. & Casciaro, S. (2013). *World J. Radiol.* **5**, 411.
Claudon, M., Cosgrove, D., Albrecht, T., Bolondi, L., Bosio, M., Calliada, F., Correas, J. M., Darge, K., Dietrich, C., D'Onofrio, M., Evans, D. H., Filice, C., Greiner, L., Jäger, K., **Jong, Nd**, Leen, E., Lencioni, R., Lindsell, D., Martegani, A., Meairs, S., Nolsøe, C., Piscaglia, F., Ricci, P., Seidel, G., Skjoldbye, B., Solbiati, L., Thorelius, L., Tranquart, F., Weskott, H. P. & Whittingham, T. (2008). *Ultraschall Med.* **29**, 28–44.
Gregg, C. L. & Butcher, J. T. (2012). *Differentiation*, **84**, 149–162.
Honda, Y. (2003). *Oral Radiol.* **19**, 14–21.
Huang, J., Yu, J. & Peng, Y. (2016). *Oncol. Lett.* **11**, 3522–3526.
Jamison, R. A., Dubsky, S., Siu, K. K., Hourigan, K. & Fouras, A. (2011). *Ann. Biomed. Eng.* **39**, 1643–1653.
Kim, S. H., Lee, J. H., Hyun, H., Ashitate, Y., Park, G., Robichaud, K., Lunsford, E., Lee, S. J., Khang, G. & Choi, H. S. (2013). *Sci. Rep.* **3**, 1198.
Lee, S. J., Park, H. W. & Jung, S. Y. (2014). *J. Synchrotron Rad.* **21**, 1160–1166.
Lewis, R. A. (2004). *Phys. Med. Biol.* **49**, 3573–3583.
Lundström, U., Westermark, U. K., Larsson, D. H., Burvall, A., Arsenian Henriksson, M. & Hertz, H. M. (2014). *Phys. Med. Biol.* **59**, 2801–2811.
Millard, T. P., Endrizzi, M., Everdell, N., Rigon, L., Arfelli, F., Menk, R. H., Stride, E. & Olivo, A. (2015). *Sci. Rep.* **5**, 12509.
Qi, X., Yang, Y., Jack, N., Santhanam, A., Yang, L., Chen, A. & Low, D. (2016). *Med. Phys.* **43**, 3409.
Sciallero, C., Balbi, L., Paradossi, G. & Trucco, A. (2016). *R. Soc. Open Sci.* **3**, 160063.
Snigirev, A., Snigireva, I., Kohn, V., Kuznetsov, S. & Schelokov, I. (1995). *Rev. Sci. Instrum.* **66**, 5486–5492.
Tang, R., Chai, W. M., Yan, F., Yang, G. Y. & Chen, K. M. (2016). *Eur. Radiol.* **26**, 3253–3261.
Tang, R., Li, W. X., Huang, W., Yan, F., Chai, W. M., Yang, G. Y. & Chen, K. M. (2013). *Sci. Rep.* **3**, 2313.
Tang, R., Xi, Y., Chai, W. M., Wang, Y., Guan, Y., Yang, G. Y., Xie, H. & Chen, K. M. (2011). *Phys. Med. Biol.* **56**, 3503–3512.
Tang, R., Yan, F., Yang, G.-Y. & Chen, K.-M. (2017). *J. Synchrotron Rad.* **24**, 1260–1264.
Wilkins, S. W., Gureyev, T. E., Gao, D., Pogany, A. & Stevenson, A. W. (1996). *Nature (London)*, **384**, 335–338.
Xi, Y., Tang, R., Wang, Y. & Zhao, J. (2011). *Appl. Phys. Lett.* **99**, 011101.
Zhang, X. C., Yang, Z. G., Li, Y., Min, P. Q., Guo, Y. K., Deng, Y. P. & Dong, Z. H. (2008). *Abdom. Imaging*, **33**, 689–694.